Processes of virtual cathodes interaction in multibeam system

Artem A. Badarin, Semen A. Kurkin, Alexey A. Koronovskii, Alexander E. Hramov, and Alexey O. Rak

Citation: Physics of Plasmas **25**, 083110 (2018); doi: 10.1063/1.5040505
View online: https://doi.org/10.1063/1.5040505
View Table of Contents: http://aip.scitation.org/toc/php/25/8
Published by the American Institute of Physics

Processes of virtual cathodes interaction in multibeam system

Artem A. Badarin,[1,2] Semen A. Kurkin,[1,2] Alexey A. Koronovskii,[1] Alexander E. Hramov,[2,a)] and Alexey O. Rak[3]
[1]*Saratov State University, 83 Astrakhanskaya str., Saratov 410012, Russia*
[2]*Saratov State Technical University, 77 Politechnicheskaya str., Saratov 410054, Russia*
[3]*Belarusian State University of Informatics and Radioelectronics, 6 P. Brovki str., Minsk 220013, Belarus*

(Received 17 May 2018; accepted 30 July 2018; published online 16 August 2018)

Two variants of schemes of a multibeam vircator are proposed and studied in this paper. Numerical analysis of the influence of various parameters of these systems (magnitude of the external magnetic field and detuning of beam currents) on the generation characteristics was conducted. The possibility of synchronizing several virtual cathodes in a single drift space of a multibeam vircator is demonstrated. The regime maps of basic control parameters of the system are built. The possibility of effective interaction of several virtual cathodes in a single drift space is analyzed, and the conditions for implementing an effective addition of powers of each beam at the output load are determined. *Published by AIP Publishing.* https://doi.org/10.1063/1.5040505

I. INTRODUCTION

Virtual cathode (VC)-based generators (vircators, reditrons, virtodes, etc.) are one of the most popular devices of high-power vacuum microwave electronics[1–3] and are currently actively studied.[4–9] Their principle of operation is based on the formation in a vacuum tube of a high-density oscillating virtual cathode (VC) in electron beam, with VC oscillations exciting microwave radiation.[10] One of the main advantages of devices that are based on a virtual cathode is the possibility of generating high-power electromagnetic radiation using a simple device design. The disadvantages are low efficiency (usually about 1%–3%) and a relatively low generation frequency.

A possible method for increasing the operating frequency of vircator systems is to increase density of the injected electron beam. Note that the generation frequency of this type of device is directly proportional to the plasma frequency of the injected electron beam, which is determined by its density. Nevertheless, the frequency increase usually leads to a sharp decrease in generation power because, in all known vircator schemes, there exists an optimum value of the injected current.[4,6,11] This makes the use of this method unacceptable for the significant increase in frequency.

A possible solution to the problem of the vircator generation frequency increase is to develop new generator schemes that are based on a virtual cathode.[11–15] Specifically, this paper describes the development and analysis of a multibeam vircator system. Thus, the idea of creating several VCs in the vircator drift space (by injecting several electron beams with supercritical currents) to increase power of higher-frequency spectral components via the interaction (synchronization) between VCs seems promising. Note that multibeam schemes are widely used in microwave electronics.[6] For example, currently, multibeam klystrons are widespread.[16–18] Several electron beams in klystrons are used instead of one to improve the electron beam grouping and, consequently, efficiency.

Note that multibeam vircator systems have been previously investigated in Ref. 19, and this scheme has demonstrated the possibility of essential efficiency enhancement. However, the issues related to the possibility of increasing the generation frequency in such a system in cases when the currents of individual beams are different have not yet been considered. Therefore, it is important to study them from a fundamental point of view. Analysis of such systems raises a number of questions, and this paper aims to answer them. Specifically, is it possible to have an effective interaction between several virtual cathodes in a single drift space to generate higher-frequency spectral components? What are the conditions for effective addition of powers of each beam at the output load? What is the spectral composition of the output radiation? Are there new physical phenomena observed in the system under consideration?

II. MULTIBEAM VIRCATOR DESIGN AND NUMERICAL MODEL

A three-dimensional particle-in-cell (PIC) electromagnetic code was used to simulate complex non-stationary processes of electron-wave interaction in the beam-plasma system studied.[20]

Two models of the relativistic multibeam vircator are considered in this paper: with 3 and 4 electron beams, which are schematically represented in Fig. 1. The models studied represent a drift space in the form of a cylindrical waveguide segment [see Fig. 1(c)], into which $N = 3$ or $N = 4$ solid relativistic electron beams with currents I_n (where n is the beam number) and energy W_e each are injected. The positions of injection regions of the electron beams (emitters) are chosen symmetrically relative to the symmetry axis of the system [see Fig. 1(a)]. The electromagnetic energy is output through a coaxial waveguide that is connected to the output part of the system, which is simulated using a waveguide port. The geometrical parameters of the model are as follows: drift space length $L = 45$ mm, drift space radius $R_w = 12$ mm, and radius of one electron beam $r = 2$ mm. The system is in an

a)Electronic mail: kurkinsa@gmail.com

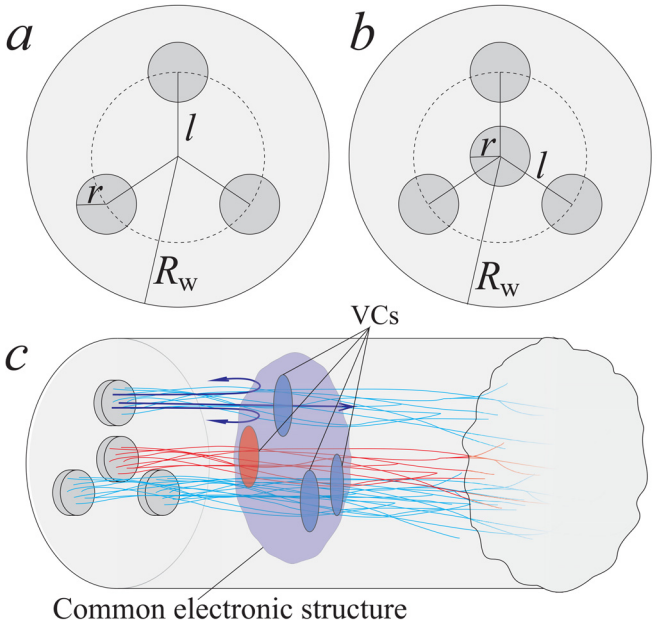

FIG. 1. Qualitative representation of the model of the multibeam relativistic vircator system [(a) and (b)—cross-sections of the three- and four-beam vircator, respectively, (c)—three-dimensional representation of the model). Figure (c) shows a segment of cylindrical drift chamber of radius $R = 12$ mm, into which 4 solid cylindrical electron beams of radii $r = 2$ mm each are injected. The areas of virtual cathodes are also schematically depicted in the figure *c* for clarity, with the red color shows the base VC and the blue—the additional ones. The big blue shape depicts a common electronic structure formed by individual virtual cathodes.

external focusing longitudinal uniform magnetic field with induction B. At the same time, the geometric dimensions of the waveguide were chosen to reduce the influence of the electrodynamic system eigenmodes on beam dynamics. For this purpose, the diameter of the drift space was set much larger in relation to the characteristic wavelength of the wave processes occurring in the vircator.

We emphasize that virtual cathodes are shown separately in Fig. 1(c) for clarity, although in reality they form via the space-charge field a common electronic structure.

III. RESULTS OF THE MULTIBEAM VIRCATOR STUDY

The virtual cathode synchronization effect was discovered in the numerical study of the proposed models for the first time. To demonstrate this effect, consider Fig. 2. The figure shows the normalized power spectra of the signal at the waveguide port output when one electron beam is injected into the system with a current of 12 kA, 14 kA, or 16 kA and when three electron beams are injected with currents of 12 kA, 14 kA, and 16 kA. It is clearly observed that an increase in the beam current leads to an increase in the fundamental generation frequency. Furthermore, with a simultaneous injection of three electron beams, generation is observed at a frequency that corresponds to a beam with a higher current. It is also seen that, in this case, power of microwave radiation significantly increases due to the imposition of oscillation frequency of the most powerful VC on less powerful beams. The output radiation power of the 3-beam system is 7 times higher than the output power of the single-beam system with

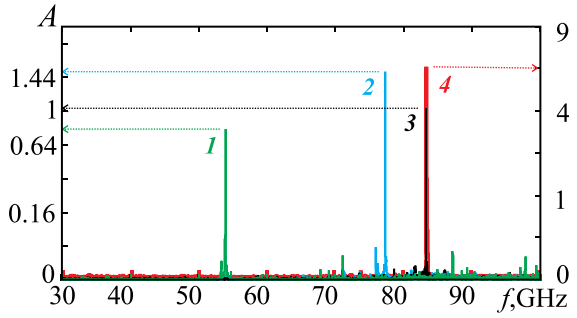

FIG. 2. The normalized power spectra of the signal at the waveguide port output in the model of multibeam relativistic vircator when one electron beam is injected into the system with a current of 12 kA (green spectrum *1*), 14 kA (blue spectrum *2*), or 16 kA (black spectrum *3*) and when three electron beams are injected with currents of 12 kA, 14 kA, and 16 kA (red spectrum *4*, right scale). The spectra are normalized to the power of the main spectral component of the output signal generated in a single-beam system with a current of 16 kA. The power scales are nonlinear (quadratic) for a better results representation. The value of the induction of an external magnetic field is $B = 1$ T; the energy of the injected electron beams $W_e = 1$ MeV.

a current of 16 kA. Thus, an electron beam with higher current acts as the beam that determines the frequency, and beams with lower currents additionally feed the system.

The influence of beam current detuning values on system dynamics was studied. Specifically, one of the electron beams was chosen as the "base" beam, with respect to which the current detuning values of other beams δ_1, δ_2 were measured. They are determined as follows: $\delta_n = I_n/I_0 - 1$, where I_n is the current of the n-th beam and I_0 is the current of the "base" beam. The current detuning magnitude ranged from –0.6 to 0 for the two "base" beam current values: $I_0 = 5$ kA and 10 kA. Strong influence of current detuning values of electron beams on the system dynamics is observed, with a general tendency that the system dynamics regime becomes more complex with the increase in the difference between detuning values. In addition, regions with single-frequency generation are observed, which are caused by the suppression of all frequencies by the one frequency.

For a more detailed analysis of the influence of beams current detuning values, the characteristic regimes of system dynamics were distinguished in the parameter plane (δ_1, δ_2) [see Figs. 3(a) and 3(b)]. These regimes differ in the number of intensive components in the Fourier power spectrum of the output signal (here, intensive components mean those that overcome the 10% barrier of the maximum spectral component amplitude). Specifically, "Regime 1" is single-frequency, "Regime 2" is dual-frequency, "Regime 3" is triple-frequency, and "Regime 4" is a regime when more than three intensive components are observed in the output signal spectrum.

Note that when analyzing the influence of beams current detunings on system dynamics, one should take into account both the magnitude of the additional beams currents detunings from the base and detuning between the additional beams. Therefore, we introduce a parameter $\delta = \delta_2 - \delta_1$, which is equal to the difference between detuning values of additional beams and the two-dimensional "detuning vector" $\vec{\Delta}(\delta_1, \delta_2)$, the length of which characterizes the total detuning of additional beams from the base and is defined as

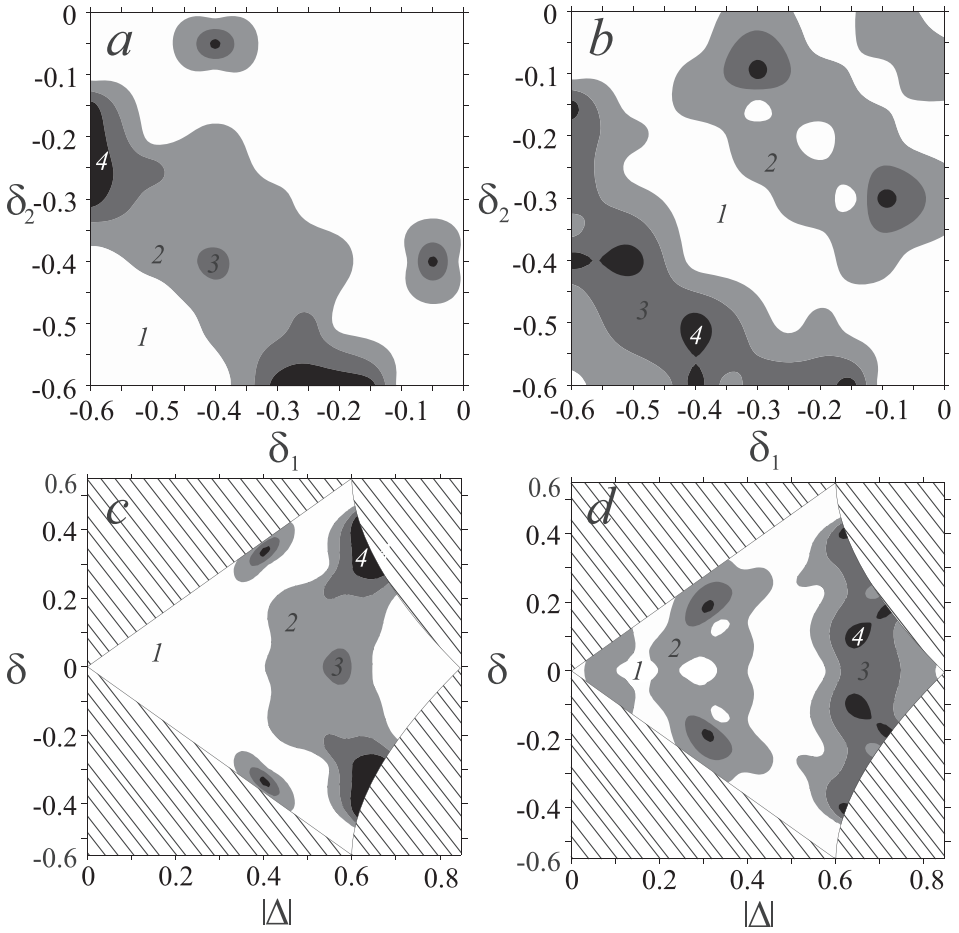

FIG. 3. Maps of characteristic regimes of the vircator system with three electron beams in the parameter planes (δ_1, δ_2) and ($|\Delta|, \delta_2 - \delta_1$), where δ_1 and δ_2—current detuning values of additional beams relative to the base beam, $|\Delta|$—length of the detuning vector. The following regimes have been distinguished, differing in the number of intensive components in the Fourier power spectrum of the output signal: 1—single-frequency, 2—dual-frequency, 3—triple-frequency, 4—regime when more than three intensive components are observed in the output signal spectrum. Maps (a) and (c) have been built for base beam current $I_0 = 5$ kA, (b) and (d)—for $I_0 = 10$ kA. The shaded regions on the fragments (c) and (d) do not have correspondence on the maps (a) and (b) because of the coordinate transformation.

$|\Delta| = \sqrt{\delta_1^2 + \delta_2^2}$. We rebuild Figs. 3(a) and 3(b) in the new coordinates $(|\Delta|, \delta)$ and analyze the system dynamics in detail.

We fix $\delta = 0$ and consider Fig. 3(c), which shows the regime map that is constructed at the current of the base beam $I_0 = 5$ kA. It is clearly seen that for the detuning vector length of $|\Delta| < 0.4$, a single-frequency mode is implemented in the system, which is characterized by the establishment of synchronous dynamics between all VCs in the beams. Increasing $|\Delta| > 0.4$ leads to the fact that system dynamics becomes more complex, and a dual-frequency regime develops. This is due to the fact that synchronization between additional beams becomes possible with the increase in total detuning of additional beams from the base (parameter $|\Delta|$) and maintenance of low detuning between additional beams (parameter δ). In this case, we can talk about the coexistence of not three, but, in fact, two virtual cathodes that oscillate with different frequencies in the system. Further increase in $|\Delta|$ leads to implementation of "Regime 3" in a small region of the control parameters [see region 3 for $|\Delta| \sim 0.58$ in Fig. 3(c)]. Then, system dynamics is successively simplified all the way to synchronization of all VCs and establishment of a single-frequency regime for $|\Delta| > 0.63$.

When the base beam current $I_0 = 10$ kA [see Fig. 3(d)], the regime map structure becomes more complicated. In particular, in the range of $0.05 < |\Delta| < 0.1$ and $0.2 < |\Delta| < 0.4$, the regions appear to be characterized by a more complex, non-single-frequency dynamics. Nevertheless, in qualitative terms, the structure of regime maps, which are depicted in Figs. 3(c) and 3(d), remains similar. In particular, for $|\Delta| \sim 0.65$ and $\delta \sim \pm 0.4$, and for $|\Delta| \sim 0.35$ and $\delta \sim \pm 0.3$, the most complex regimes are implemented in both cases.

Now, we fix $|\Delta| = 0.32$ and begin to increase detuning δ between additional beams at the base current $I_0 = 10$ kA [see Fig. 3(d)]. First (for $\delta \sim 0$), a single-frequency synchronous regime is implemented, which is associated with the imposition by the base beam of its own dynamics on the remaining beams. Then, at $\delta = 0.05$, a dual-frequency regime is implemented in the system. At $0.1 < \delta < 0.14$, a window of periodicity (single-frequency regime) is observed because of deterioration of the interaction between additional beams due to an increase in detuning δ between them, i.e., it becomes "easier" for the base VC to impose its dynamics. A further increase in detuning leads to the sequential complication of system dynamics from "Regime 1" to "Regime 4" when detuning between the oscillation frequencies of all virtual cathodes becomes so high that synchronization between them does not occur.

Thus, all observed regimes and main trends on the regime maps in Fig. 3 are due to the following cases of interaction between electron beams with VCs: (1) the base beam imposes its own dynamics on both VCs of additional beams—"Regime 1"; (2) interaction of two synchronous VCs with the base VC, i.e., synchronization is established between the VCs of additional beams—"Regime 2"; (3) lack

of synchronization between all VCs—"Regime 3" and "Regime 4."

The next step was the analysis of the effect of external magnetic field magnitude and value of detuning of beams currents relative to the base on the output power of a multibeam relativistic vircator with 4 electron beams. The emitters were arranged in such a way that the base beam was injected along the axis of symmetry, while the other three beams were symmetric along the azimuth with respect to the first beam at a distance of $l = 4.5$ mm from it [see Fig. 1(b)]. A strong influence of the detuning value on the output characteristics of multibeam vircator generation was observed. The optimal values of control parameters (external magnetic field, detuning) were determined to achieve the maximum output power and efficiency.

Thus, Fig. 4 shows the dependence of normalized output power at the coaxial waveguide port of the system on the magnitude of external magnetic field induction and detuning of currents (here, detunings of three additional beams currents relative to the base are the same and equal δ). The dependence is normalized to the power in the case of zero detuning (when the currents of all beams are equal) for each external magnetic field value. It can be seen that two characteristic regions are distinguished in which an increase in the output power is observed.

The region I with a relatively low negative detuning in the range from -0.2 to -0.1 and medium values of external magnetic field is the most optimal. This region arises due to the effect of synchronization of virtual cathodes, when the base VC imposes dynamics on additional VCs that have smaller currents. With an increase in external magnetic field, an increase in power is observed, followed by a sharp drop and desynchronization of virtual cathodes. Maximal normalized power is achieved at $B = 0.6$ T. This occurs because magnetic field has a focusing effect on the beams, thereby increasing their density in the VC region and improving the efficiency of their interaction. However, at a relatively high magnetic field, the electron beams cease to "mix," which reduces the influence of the base beam on the additional beams and leads to a decrease in the output power.

The region II is characterized by a positive detuning and strong external magnetic field. The base beam cannot impose its dynamics due to a decrease in the interaction strength between the beams at a large magnetic field. The additional beams in this case have currents higher than the base one and impose their own dynamics to the whole system, which leads to an increase in power.

Areas of significant weakening of output power are also observed in Fig. 4. This is due primarily to the non-coherence of the radiation of individual electrons in regimes without synchronization. The radiation spectra in these regimes are characterized by a complex spectral composition.

It should be noted that among the considered schemes, the most effective scheme has four beams (one base and three additional) with parameters lying in the region I (Fig. 4).

The features of dynamics of relativistic electron beams in the four-beam vircator were analyzed. Thus, Fig. 5 shows the evolution of phase portraits in (z, p_z) coordinates over time (where, p_z is the longitudinal impulse normalized to $m_e c$, m_e is

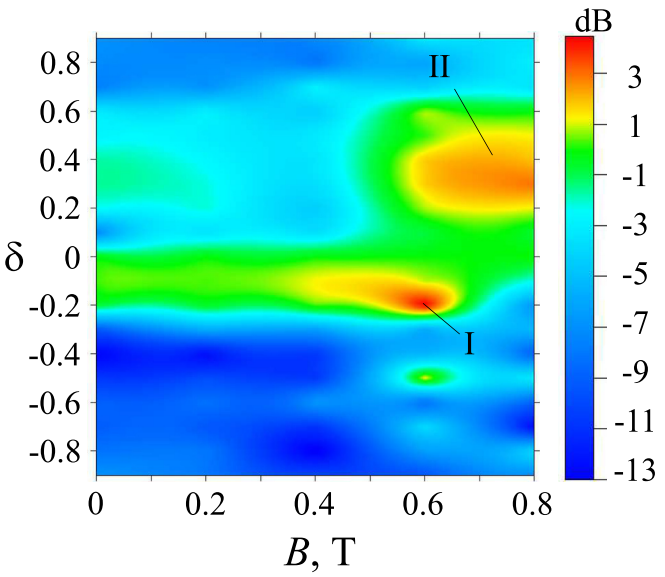

FIG. 4. The dependence of normalized output power of the four-beam vircator on the magnitude of external magnetic field induction B and detuning δ at base beam current $I_0 = 5$ kA. Detunings of three additional beams currents relative to the base are the same and equal δ. The dependence is normalized to the power in the case of zero detuning (δ) for each external magnetic field value. Roman numerals denote two characteristic regions of power increase. In region I, the main spectral component is about 65 GHz. In Region II, the radiation frequency depends on the detuning value and lies in the range 65–78 GHz.

the electron rest mass, c is the speed of light, and z is the longitudinal coordinate). It is clearly seen that two VCs exist in the system. The first VC (VC_1) corresponds to the base electron beam, and the second VC (VC_2) corresponds to the additional beams (see Fig. 5 at time $t = 2.155$ ns). Note that the VC_2 is more extended and is formed further along the z-axis, compared with the VC_1. This is due to the well-known property of the electron beam dynamics with a VC: the greater the current density of the injected beam, the closer VC is formed to the injection plane.[6]

In the following time points, up to $t = 2.165$ ns, both VCs (VC_1 and VC_2) accumulate charge, which increases the space charge density, while the average position of VC of the base beam moves to the right along the z-axis. At the same time, the position of VCs of the additional beams shifts to the left. At $t = 2.165$ ns, both VCs become localized at approximately one point along the z-axis. Furthermore, VCs begin to discharge the accumulated charge, which forms dense electron bunches that move further into the drift space, and this effect is more pronounced for the base beam. Such dynamics in the system studied is observed when a synchronous regime is established. We also note that the amplitude of VC oscillations increases with time, and Fig. 5 only shows one VC oscillation period at early time points. Thus, VC_2 acts as an active medium (distributed VC[21]) which contributes to an increase in the amplitude of the oscillations of the first VC due to the synchronous interaction between them, with the oscillation frequency being set by the VC_1.

IV. DISCUSSION AND CONCLUSIONS

This paper provides a numerical study of nonlinear dynamics of a multibeam vircator system. The multibeam

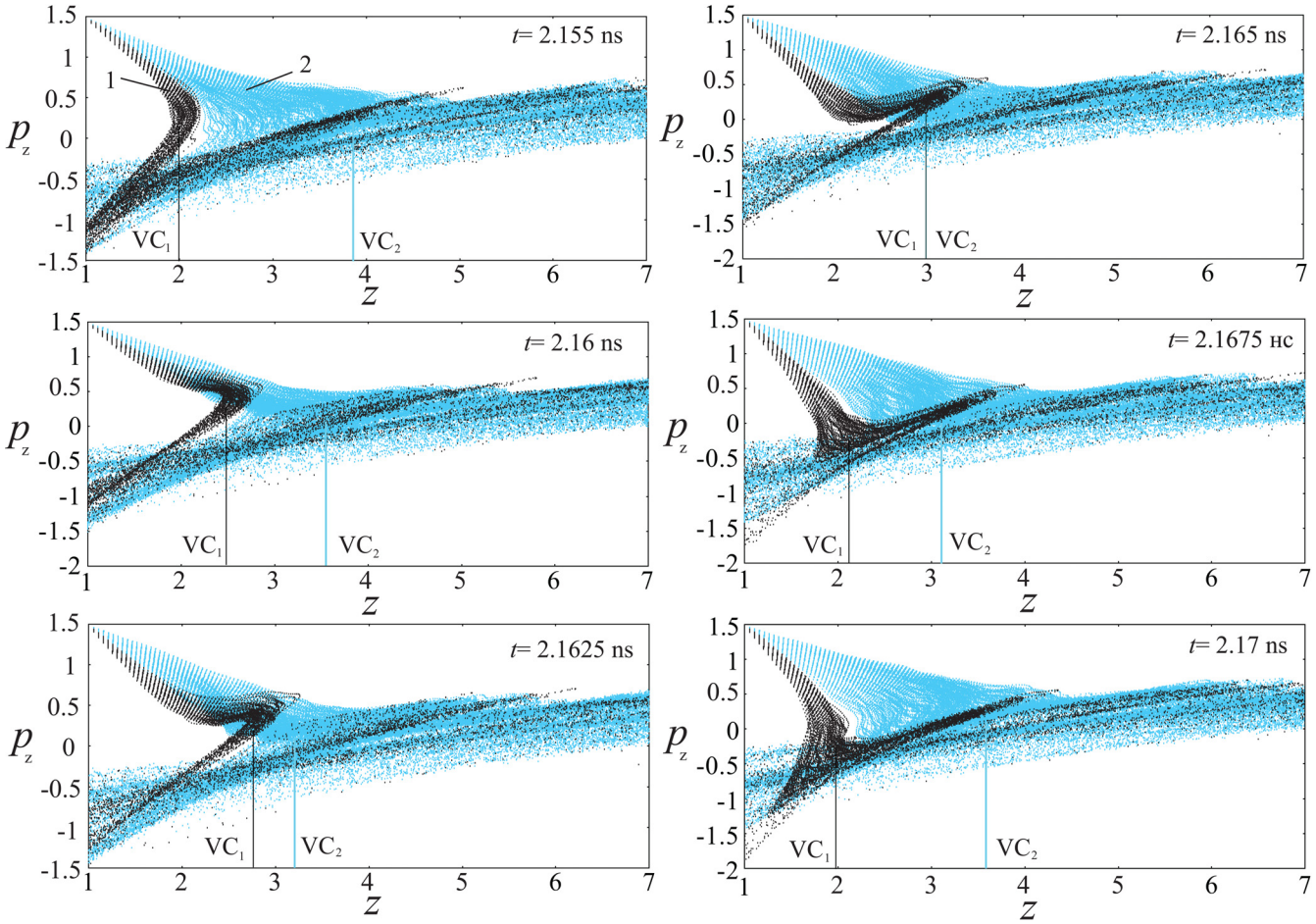

FIG. 5. The evolution of phase portraits over time within one period of VC oscillations. Here, p_z is the longitudinal impulse normalized to $m_e c$, m_e is the electron rest mass, c is the speed of light, and z is the longitudinal coordinate. Black color and the number *1* correspond to the base electron beam; blue color and the number 2—to the additional beams. The current of the base beam is $I_0 = 5$ kA, detuning of additional beams from the base $\delta = -0.63$, frequency of the main spectral component is 65 GHz.

vircator scheme with detuned electron beams has not been previously considered. The possibility of effective interaction of several virtual cathodes in a single interaction space was analyzed as part of numerical simulation, and conditions of effective addition of powers of each beam at the output load were determined. The effect of synchronization of virtual cathodes in the model of a multibeam relativistic vircator was discovered for the first time. This effect is important both from the fundamental and applied points of view because it can allow shifting relativistic vircators to a higher frequency range without substantially increasing the total current in the system. This result can be achieved using one relativistic electron beam with the highest current as the beam that determines the frequency, and the remaining $(N - 1)$ beams with lower currents as supporting beams, which "pump" the necessary energy into the system. Thus, to increase the vircator generation frequency (which is determined by the plasma frequency) and the power at a given frequency, it is not necessary to increase the total current injected into the system, compared with the single beam. However, it is sufficient to increase only the current of one of the N beams (base). As a result, due to synchronization, VCs in all electron beams will oscillate at one frequency, which is set by the VC oscillations frequency in the base beam, which will lead to an increase in the output signal power at this frequency. The formed synchronously oscillating virtual cathodes can be considered as a single spatially distributed inhomogeneous electron structure.

Thus, taking into account the peculiarities of such sources of high-power microwave radiation as devices with a virtual cathode, a new scheme is proposed, a multibeam vircator system, where the addition of powers of each of the oscillating virtual cathodes occurs in a common resonator (drift chamber). In this system, several beams with supercritical currents are loaded on a common resonator. The proposed scheme is promising for further increasing the power and frequency of generators on a virtual cathode.

ACKNOWLEDGMENTS

The studies, which are associated with the development of mathematical and numerical models of the system studied, were performed with the support of the Ministry of Education and Science of the Russian Federation (Project 3.859.2017/4.6). The synchronization effects of several virtual cathodes in a multibeam vircator system were studied in detail with the support of the Russian Foundation for Basic Research (Grant No. 17-52-04097). A.E.H. acknowledges individual financial

support from the Ministry of Education and Science of the Russian Federation (Project 3.4593.2017/6.7).

[1]R. A. Mahaffey, P. A. Sprangle, J. Golden, and C. A. Kapetanakos, "High-power microwaves from a non-isochronous reflecting electron system," Phys. Rev. Lett. **39**, 843 (1977).
[2]A. N. Didenko, Ya. Krasik, S. P. Perelugin, and G. P. Fomenko, "Generation of power microwave radiation of relativistic beam in triode system," Tech. Phys. Lett. **5**, 321 (1979).
[3]A. E. Dubinov and V. D. Selemir, "Electronic devices with virtual cathodes (review)," J. Commun. Technol. Electron. **47**, 575 (2002).
[4]A. S. Shlapakovski, T. Queller, Yu. P. Bliokh, and Ya. E. Krasik, "Investigations of a double-gap vircator at sub-microsecond pulse durations," IEEE Trans. Plasma Sci. **40**, 1607–1617 (2012).
[5]S. A. Kurkin, A. E. Hramov, and A. A. Koronovskii, "Microwave radiation power of relativistic electron beam with virtual cathode in the external magnetic field," Appl. Phys. Lett. **103**, 043507 (2013).
[6]J. Benford, J. A. Swegle, and E. Schamiloglu, *High Power Microwaves*, 3rd ed., Series in Plasma Physics (CRC Press/Taylor and Francis Group, 2016).
[7]A. E. Hramov, A. A. Koronovsky, S. A. Kurkin, and I. S. Rempen, "Chaotic oscillations in electron beam with virtual cathode in external magnetic field," Int. J. Electron. **98**, 1549–1564 (2011).
[8]S. A. Kurkin, N. S. Frolov, A. O. Rak, A. A. Koronovskii, A. A. Kurayev, and A. E. Hramov, "High-power microwave amplifier based on overcritical relativistic electron beam without external magnetic field," Appl. Phys. Lett. **106**, 153503 (2015).
[9]J. Ju, D. Cai, G. Du, Y. Wang, L. Liu, and J. Zhang, "Characterization of cesium iodide-coated carbon-fiber aluminum cathode for an s-band high-efficiency vircator," IEEE Trans. Plasma Sci. **43**, 3522–3526 (2015).
[10]L. Thode, B. B. Godfrey, and W. R. Shanahan, "Vacuum propagation of solid relativistic electron beams," Phys. Fluids **22**, 747–763 (1979).
[11]N. S. Frolov, S. A. Kurkin, A. A. Koronovskii, and A. E. Hramov, "Nonlinear dynamics and bifurcation mechanisms in intense electron beam with virtual cathode," Phys. Lett. A **381**, 2250–2255 (2017), ISSN 0375-9601.
[12]A. E. Dubinov, A. G. Petrik, S. A. Kurkin, N. S. Frolov, A. A. Koronovskii, and A. E. Hramov, "Virpertron: A novel approach for a virtual cathode oscillator design," Phys. Plasmas **24**, 073102 (2017).
[13]S. A. Kurkin, A. A. Badarin, A. A. Koronovskii, and A. E. Hramov, "The development and interaction of instabilities in intense relativistic electron beams," Phys. Plasmas **22**, 122110 (2015).
[14]S. A. Kurkin, A. A. Koronovskii, and A. E. Hramov, "Effect of the electron beam modulation on the sub-THz generation in the vircator with the field-emission cathode," J. Plasma Phys. **81**(3), 905810320 (2015).
[15]S. A. Kurkin, A. A. Badarin, A. A. Koronovskii, and A. E. Hramov, "Higher harmonics generation in relativistic electron beam with virtual cathode," Phys. Plasmas **21**, 093105 (2014).
[16]D. Liu, M. Xie, Y. Cheng, H. Wang, and C. Yuan, "Numerical study of a multibeam klystron on the milky way high-performance computing platform," IEEE Trans. Electron Devices **64**, 1857–1860 (2017).
[17]A. Y. Baikov, C. Marrelli, and I. Syratchev, "Toward high-power klystrons with rf power conversion efficiency on the order of 90%," IEEE Trans. Electron Devices **62**, 3406–3412 (2015).
[18]Z. Liu, H. Huang, X. Jin, and L. Lei, "Design of an x-band gigawatt multibeam relativistic klystron amplifier," IEEE Trans. Plasma Sci. **42**, 3419–3422 (2014).
[19]M. Sumathy, S. K. Chhotray, D. Senthil Kumar, K. S. Bhat, and L. Kumar, "Analysis of a multibeam vircator configuration for efficiency enhancement," IEEE Trans. Plasma Sci. **37**, 293–297 (2009).
[20]C. K. Birdsall and A. B. Langdon, *Plasma Physics via Computer Simulation* (Taylor and Francis Group, 2005).
[21]A. E. Dubinov, A. G. Petrik, S. A. Kurkin, N. S. Phrolov, A. A. Koronovskii, and A. E. Hramov, "Beam-plasma instability in charged plasma in the absence of ions," Phys. Plasmas **23**, 042105 (2016).